JOURNAL OF MAGNETIC RESONANCE **135,** 194–202 (1998)
ARTICLE NO. MN981578

Evaluating Human Breast Ductal Carcinomas with High-Resolution Magic-Angle Spinning Proton Magnetic Resonance Spectroscopy

Leo Ling Cheng,*,†,[1] I-Wen Chang,† Barbara L. Smith,‡ and R. Gilberto Gonzalez†

Department of Pathology, †NMR Center, Department of Radiology, ‡Division of Surgical Oncology, Massachusetts General Hospital, Harvard Medical School, Boston, Massachusetts 02129

Received March 24, 1998; revised August 4, 1998

We report the results of a study of human breast ductal carcinomas, conducted by using high resolution magic angle spinning proton magnetic resonance spectroscopy (HRMAS 1HMRS). This recently developed spectroscopic technique can measure tissue metabolism from intact pathological specimens and identify tissue biochemical changes, which closely correspond to tumor *in vivo* state. This procedure objectively indicates diagnostic parameters, independent of the skill and experience of the investigator, and has the potential to reduce the sampling errors inherently associated with procedures of conventional histopathology. In this study, we measured 19 cases of female ductal carcinomas. Our results demonstrate that: (1) highly resolved spectra of intact specimens of human breast ductal carcinomas can be obtained; (2) carcinoma-free tissues and carcinomas are distinguishable by alterations in the intensities and the spin–spin relaxation time T2 of cellular metabolites; and (3) tumor metabolic markers, such as phosphocholine, lactate, and lipids, may correlate with the histopathological grade determined from evaluation of the adjacent specimen. Our results suggest that biochemical markers thus measured may function as a valuable adjunct to histopathology to improve the accuracy of and reduce the time frame required for the diagnosis of human breast cancer.

Key Words: **proton magnetic resonance spectroscopy; high-resolution magic-angle spinning; metabolite diagnostic markers; human breast ductal carcinomas; intact tissue specimens.**

INTRODUCTION

Due to increased public interest, gains achieved through mammography, and the continuing development of breast screening techniques (*1–12*), breast cancer, representing 31% of all new cancer cases, is currently the most frequently diagnosed cancer in American women. The progress in breast cancer diagnosis, however, also reflects the staggering incidence of the disease: breast cancer is, in fact, the second most frequent cause of cancer death (17% of cancer deaths) among women in the U.S., following lung cancer at 25%, and ahead of colon and rectal at 10% (*13*).

As with many other malignant diseases, success in breast cancer management and patient outcome, including survival and quality-of-life, greatly depends on early detection of the lesion (*14*). However, diagnostic accuracy with respect to tumor type and grade is also crucial to the selection of optimal treatment modalities (*15*). In the past decade, biomedical engineering efforts have emphasized the development of techniques for detecting abnormalities in the breast, and indisputable successes have been achieved. The development of improved methods for the pathology assessment of tumor type and grade, however, has met with less than proportional success.

When a suspicious breast lesion is detected, surgical biopsy is generally performed to obtain a tissue specimen, followed by pathological assessment of observable changes in cellular morphology, including type and grade for lesions deemed cancerous. Based on the pathology report, a treatment plan is proposed, and may include a modified radical mastectomy or breast-conserving surgery. Following surgery, pathologists again evaluate the excised tumor, along with the removed axillary lymph nodes, to look for signs of metastasis. The final pathology report, based on any detectable lymph node metastasis, is used to guide post-surgical therapy and overall patient management (*16–21*).

Unfortunately, histopathology evaluations are limited by their labor-intensive character and, as a result, only a small amount ($<1 \sim 2\%$) of the surgically excised tumors and lymph nodes are microscopically examined. These limits raise the issue of sampling error, especially given the well-described heterogeneity of tumors. Furthermore, the characteristics upon which the histopathological examination relies are descriptive in nature, and so remain subject to observer interpretation. For this reason, the pathology report, and thus the prognostic opinion, heavily depends upon the experience of the pathologist. Studies have shown that 30% of breast cancer patients diagnosed with negative lymph node involvement at the time of surgery develop metastatic disease within 5 years, implying that nodal micro-metastases, not obvious during routine histopathology, may play a critical role in patient survival (*16*).

The altered cellular metabolism exhibited by tumors (*22–*

[1] Reprint requests should be addressed to Leo L. Cheng, Ph.D., Pathology Research, MGH, CNY-7, 149 13th Street, Charlestown, MA 02129. E-mail: cheng@nmr.mgh.harvard.edu.

1090-7807/98 $25.00

24), possibly prior to observable morphological changes (*25*), may provide a less subjective means of identifying the presence of cancer within primary sites and metastases to other regions (*26*). Local biochemical changes, and thus tumor metabolic alterations, can be detected by proton magnetic resonance spectroscopy (1HMRS). A decade of worldwide attempts to use *ex vivo* conventional solution 1HMRS for the analysis of intact specimens and tissue extracts has achieved success in identifying 1HMRS detectable malignancy associated metabolic alterations; however, clinically applicable protocols have thus far not yielded from those attempts.

The difficulty of analyzing intact tissues with solution MR methods is the direct result of the inherent difference in characteristics between heterogeneous tissues and homogeneous solutions. Due to the restricted molecular motions in tissues and magnetic susceptibility, tissue 1HMR spectra obtained with conventional techniques are generally broad, have low spectral resolution, and are limited in their ability to differentiate individual resonance. A variety of approaches aimed at improving the utility of intact tissue 1HMRS have been proposed and tested within the framework of conventional solution MR technology (*27–36*). Some of these techniques have demonstrated advantages over routine histopathological evaluations, such as detection of micro-metastases (*25*). However, owing directly or indirectly to inadequate spectral resolution, the overall clinical usefulness remains compromised by an inability to differentiate between individual metabolites and to correlate metabolites with disease states.

Different problems arise in the analysis of extracts. Conventional solution 1HMRS techniques are designed to analyze bulk homogeneous solution and, when applied to measurements of solutions obtained from tumor extracts, produce proton MR spectra with high resolution. However, the extraction procedures alter the measured water soluble metabolites to unknown degrees from their intact states (*37*). Consequently, studies have shown that 1HMR measurement of tumor metabolites in extraction solutions may not correlate with pathological observation, even when the laborious extraction procedures can be tolerated in clinical laboratories (*22*).

High-resolution magic-angle spinning (HRMAS) 1HMRS is capable of analyzing the cellular metabolism of surgically removed intact tissue at a high spectral resolution. By using this method, we have shown that high spectral resolution, previously observed only with aqueous solutions, can be obtained with intact tissue (*38*). Our findings have now been corroborated by other research groups (*39–41*). More recently, we have also shown that metabolite intensities measured with HRMAS 1HMRS can be correlated significantly with disease states (*37, 42*).

Here, we wish to report the results and clinical implications of our investigation of a group of female breast ductal carcinomas by using HRMAS 1HMRS. Based on the analysis of high-resolution tissue spectra, we were able to determine individual tumor metabolites, investigate correlations between cellular metabolites and tumor grades determined by routine histopathological evaluation of the adjacent specimen, and estimate metabolic spin–spin relaxation time (T2). Our results demonstrate the potential and clinical relevance of this novel spectroscopic method as a valuable and objective adjunct to the investigation of tumor pathology which may result in improved accuracy in breast cancer diagnosis.

RESULTS

HRMAS Proton MR Spectra of Breast Tumors

Figure 1 compares proton MR spectra of human breast cancer and cancer-free (see details under Experimental) tissues obtained with and without the use of the HRMAS technique. The HRMAS spectra for both specimens demonstrate superior spectral resolution. Figures 1a and 1b show 1HMR spectra obtained from a cancer specimen of a 67-year-old patient diagnosed with grade II infiltrating ductal carcinoma. Both spectra were acquired with the same tissue sample and under similar experimental conditions, except that spectrum 1a was measured with HRMAS, while spectrum 1b was measured after the completion of spectrum 1a and with a conventional non-HRMAS 5-mm NMR probe. In addition, conventional 5-mm measurement of cancer tissue from the same patient before the HRMAS procedure revealed similar spectra as that of spectrum 1b (results not shown). This consistency suggests that the enhancement of spectral resolution in spectrum 1a is due to the effect of magic-angle spinning. Since human breasts are extremely rich in lipid, 1HMR spectra of breast specimens are highly likely to be obscured by fat contamination. However, Fig. 1c, a HRMAS proton MR spectrum of breast specimens obtained from the margin of resection of the same patient, shows a spectral region from 3.0 to 4.2 ppm that is free of lipid contamination. Therefore, to minimize the influence of both lipids and tissue water on spectral analysis, we concentrate our attention on this region (3.0 to 4.2 ppm), which is free of lipid and water contamination. Also in this region, we clearly observe cellular metabolites that may be cancer related, as shown in Fig. 1a.

Comparison between Malignant and Healthy Non-fatty Breast Tissue

The influence of adipose tissue on the spectrum of human breast specimens is known to be substantial, as the female human breast is known to be rich in adipose tissue. To complicate matters further, all tumors, including breast tumors, are heterogeneous. Both of these characteristics are demonstrated in Figure 2a, which shows a HRMAS 1HMR spectrum of a grade III invasive ductal carcinoma obtained from a 33-year-old patient. Comparing the spectrum of Fig. 2a with that of Fig. 1a, Fig. 2a clearly shows a much higher lipid content in the specimen and a significantly different metabolic profile as displayed by the inserted vertical amplified spectrum of the above mentioned spectral region of

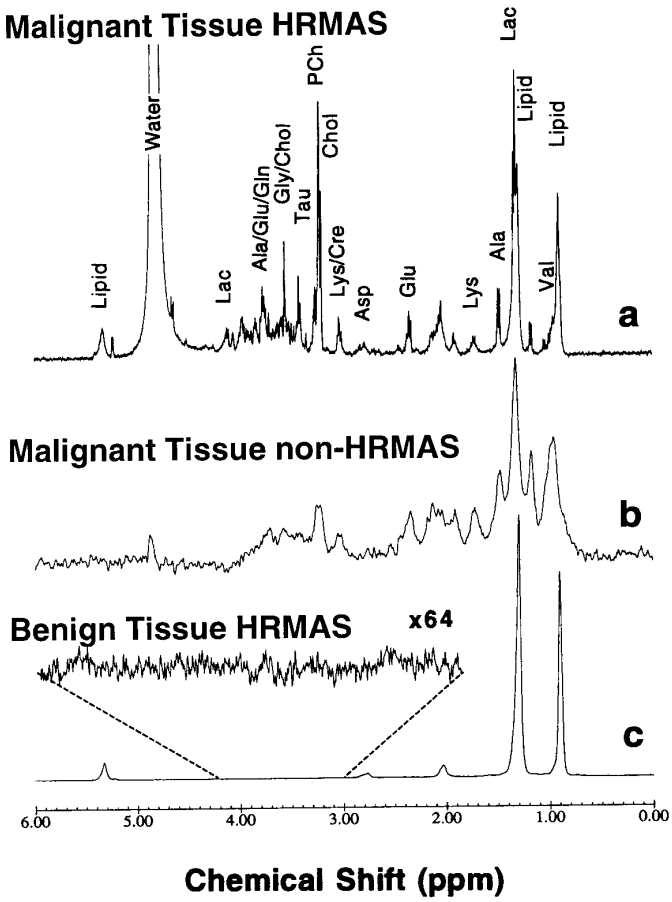

FIG. 1. Comparison of proton MR spectra of human breast tumor and non-tumor specimens obtained with and without HRMAS. Specimens were obtained from a patient diagnosed with grade II infiltrating ductal carcinoma. (a) Spectrum of intact carcinoma tissue acquired with T2-weighted HRMAS at 2.5 kHz, at 20°C. (b) Spectrum of intact carcinoma tissue acquired without HRMAS, with water presaturation, and with other experimental parameters similar as those of (a) and measured after the tissue was subjected to 2.5 kHz spinning for more than 10 minutes. (c) Spectrum of non-tumor breast tissue excised from the margin of resection. This spectrum was acquired under the identical experimental conditions as those used to obtain (a). A vertical expansion of 64 times for the spectral region between 3.0 to 4.2 ppm for (c) is shown as an insert above (c). Selected metabolite resonances are labeled on the spectra (Val, valine; Lac, lactate; Ala, alanine; Lys, lysine; Glu, glutamate; Asp, aspartate; Cre, creatine; Chol, choline; PCh, phosphorylcholine; Tau, taurine; Gly, glycine).

interest. The HRMAS 1HMRS metabolic profiles seen in Fig. 2a for malignancy and Fig. 2b for healthy breast tissue differ greatly, suggesting a very different metabolism between the two. Of all the differences in cellular metabolism detectable between Figs. 2a and 2b, however, the greatest is the absence of phosphocholine (Pch) resonance in the normal tissue (Fig. 2b). It is also noteworthy that compared with specimens obtained from the margins of breast cancer resections (mostly fatty tissue as shown in Fig. 1c), a distinct and visible feature of this specimen (Fig. 2b) was its apparently low content of adipose tissue, which elevated the levels of metabolic resonances (in the 3.0 to 4.2 ppm region) above the detectable level. Selected metabolic intensities measured for each individual case and a summary of histopathological features for patients are listed in Table 1. Lactate (4.12 ppm) is selected because of its known association with the progression of malignancy through the formation of necrosis (*43, 44*); while the choice of Pch (3.22 ppm) is based on its known biological functions in the acceleration of cell proliferation in the presence of malignancy (*45*). Intensities of both resonances are normalized by the intensity of choline resonance at 3.20 ppm in order to evaluate spectroscopic results among cases, since the excess amount of adipose tissue in human breast specimens often prevents a meaningful estimation of the absolute metabolic intensity as determined by sample weight.

Spin–Spin Relaxation Time T2 of Lipid Metabolites

As shown in Fig. 1, many resonances observed in HRMAS 1HMRS spectra can be assigned to specific malignancy-associated metabolites and fatty acid components. More detailed

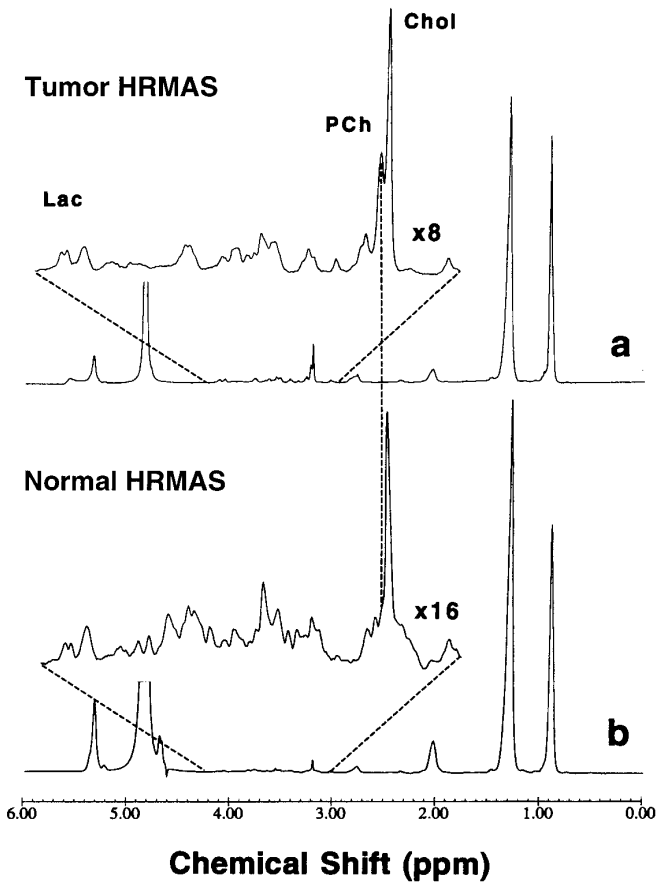

FIG. 2. Comparison between HRMAS Proton MR spectra of human ductal carcinoma and normal breast tissues. Both spectra were acquired and processed identically. (a) A grade III invasive ductal carcinoma specimen and (b) a normal specimen. Vertical expansions for the spectral region between 3.0 to 4.2 ppm of both spectra are shown as inserts with identified times of expansions. The resonances of lactate, phosphocholine, and choline used in the data analyses are labeled above the spectra.

TABLE 1
Patient Histopathological Evaluation and HRMAS 1HMRS Data

	Histopathology			HRMAS 1HMRS	
Patient age	Grade	Size (cm)	LNM	Lac/chol %	PCh/chol %
66	DCIS	ND	ND[a]	20.6	137.0
43	I	0.8	1/23	43.1	102.9
84	II	2.2	ND[b]	10.1	85.0
85	II	3.0	ND[c]	16.5	599.1
50	II	2.0	0/16	16.7	128.9
44	II	2.2	NA	14.7	95.0
65	II	2.0	ND[d]	13.8	58.6
77	II	1.0	0/11	21.1	172.4
67	II	1.7	2/22	41.6	176.5
71	II	4.0	2/12	67.6	192.6
68	II	4.0	3/12	25.6	179.9
66	II-III	0.9, 0.6[e]	0/16	35.2	39.3
70	II-III	4.5	4/15	240.2	1856.6
44	III	1.8	5/11	66.4	65.2
60	III	2.3	7/10	68.7	110.1
45	III	4.5	1/27	386.6	1577.1
65	III	3.5	0/16	161.7	807.5
36	III	1.2	0/10	NO	328.8
33	III	2.8	23/27	21.2	49.7

Note. LNM, lymph node metastasis, *X*/*Y*. *Y*, the number of lymph nodes examined; *X*, the number of lymph nodes that were positive of metastases. DCIS, ductal carcinoma-in-situ. ND, not determined. NA, not available. NO, not observed.

[a] Pure DCIS, nodes were not taken during surgical procedures.

[b] Nodes were not taken, because of the evidence of distant metastases.

[c] Nodes were not taken, because of the advanced age of the patient.

[d] Nodes were not taken, because of known metastases and multiple medical problems.

[e] Two primary tumors: multifocal grade II ~0.9 cm and grade III ~0.6 cm.

assignments were then made based on literature data and/or two-dimensional correlation spectroscopy (2D COSY) of intact tissue HRMAS spectra. By using these assignments, we were able to measure the spin–spin relaxation time (T2) of cellular metabolites and fatty acids for carcinoma and carcinoma-free specimens by varying the filter length of the CPMG sequence. Table 2 lists the T2 values determined for various components of fatty acids from the series of spectra. For cellular metabolites, the only T2s listed are phosphorylcholine (Pch, 3.22 ppm) and choline (Chol, 3.20 ppm), as shown in Fig. 2. Among the carcinoma specimens we have analyzed thus far, the intensities of Pch and Chol resonances are much higher than those of other metabolites, with the exception of those produced by fatty acids. The disproportional intensity difference between fatty acids and cellular metabolites may increase uncertainty in determinations of T2 for cellular metabolites, in addition to inherent T2 variations due to tumor heterogeneity. This may partly account for the fact that standard errors generally represent over 7% of mean T2 values for Pch and Chol, while a similar average for fatty acid components is only about 4%, as shown in Table 2.

Tissue Biostability During the Time Course of NMR Measurements

Figure 3 compares two HRMAS spectra of exactly the same malignant tissue specimen, but measured at an interval of 2 h. This interval approximates the total time required to accomplish tumor resection, sample freezing, and the completion of HRMAS measurement. Figure 3 demonstrates that, within this time frame, no measurable biochemical changes occur which can be detected with current HRMAS technique.

DISCUSSION

Owing to the extremely high content of adipose tissue in the female human breast, breast cancer specimens are considered to be the most difficult intact tissues from which to obtain useful proton MR data by using conventional techniques (*22*). Nevertheless, our results demonstrate that HRMAS can achieve superior proton MR spectral resolution of tumor metabolites, even in the presence of strong lipid resonance signals from adipose tissue. This superiority is especially evident in the spectral region of 3.0 to 4.2 ppm, where the minimal influence of lipid resonances results in a flat baseline with fatty non-cancer tissue (see Fig. 1c). On the contrary, in this spectral region, healthy non-fatty breast and ductal carcinoma tissues display resolved and varied profiles of resonances (cf. Figs. 1a and 2), reflecting their altered cellular biochemistry. Based on these metabolites, we have been able to analyze and investigate the correlations between alterations of metabolites and histopathological grades of malignancy.

Of all the alterations in cellular metabolism detected by HRMAS 1HMRS in normal tissue and ductal carcinomas, we are most interested in measuring changes of the choline-related metabolites. Choline and its high-energy metabolites comprise essential building blocks of cell biology. Moreover, elevated levels of choline and choline derivatives (such as phosphocholine), have been associated with a variety of diseases and are believed to represent accelerated cell proliferation in the presence of malignancy (*45*). Elevated levels of choline and associated metabolites are reported to produce an intensive bulk resonance between 3.2 and 3.3 ppm, demonstrated in both *in vivo* MRS studies of breast cancer (*46*) and conventional *ex vivo* MR measurements of malignant breast cells (*47–49*) and tissues (*36*). Unfortunately, neither of these approaches permitted differentiation of the underlying components producing the bulk resonance, because of the inherent limitation of spectral resolution. In this study, we demonstrated the capability of HRMAS to resolve individual resonances, permitting the evaluation of choline metabolites within the widely reported bulk resonance.

Our results, in Fig. 2, indicate that, in healthy non-fatty breast tissue, choline predominates the HRMAS spectrum, while phosphocholine (Pch) is present only at a very low concentration. However, the resonance of Pch, which was

TABLE 2
Mean and Standard Errors of T2 for Lipid Metabolites and Cholines

Resonance chemical shifts (ppm)	Normal (n = 4)		DCIS (n = 1)		II (n = 7)		II-III (n = 2)		III (n = 5)	
	Mean[a]	SE[b]	Mean	SE	Mean	SE	Mean	SE	Mean	SE
Lipids										
5.33	190.9	5.5	206.4		205.4	4.9	215.3	0.3	198.5	12.3
5.23	113.9	3.1	154.7		121.3	2.8	122.3		117.6	0.0
2.77	166.9	2.1	186.5		180.9	6.4	175.0	8.3	176.0	7.1
2.25	51.9	1.2	64.3		57.1	1.9	60.6		56.2	1.8
2.03	140.3	1.8	164.1		150.4	8.9	174.7	15.3	193.0	25.9
1.59	71.1	2.7	65.5		70.8	2.6	70.6		86.6	17.4
1.30	166.3	2.8	196.4		176.4	2.2	186.8	1.4	168.7	3.2
0.90	261.6	5.3	352.9		276.1	6.7	293.2	28.6	263.2	15.4
3.22 (Pch)	427.2		460.3		347.5	7.7	406.0	35.0	389.1	15.0
3.20 (Chol)	394.4		385.3		441.9	26.0	548.8		540.0	68.2

[a] Mean, mean of metabolite T2 in ms.
[b] SE, standard error of metabolite T2 in ms.

nearly invisible in the spectrum of healthy tissue, was evident at 3.22 ppm in all cases of ductal carcinomas. This observation agrees well with reports of phosphorus-31 NMR studies of cell-lines of human breast cancer (*48, 49*). Phosphorus NMR has determined that primary breast cancer cell-lines have a 16- to 19-fold increase of Pch above normal breast epithelial cells, and metastatic breast cancer cell-lines, an increase of 27-fold (*48*).

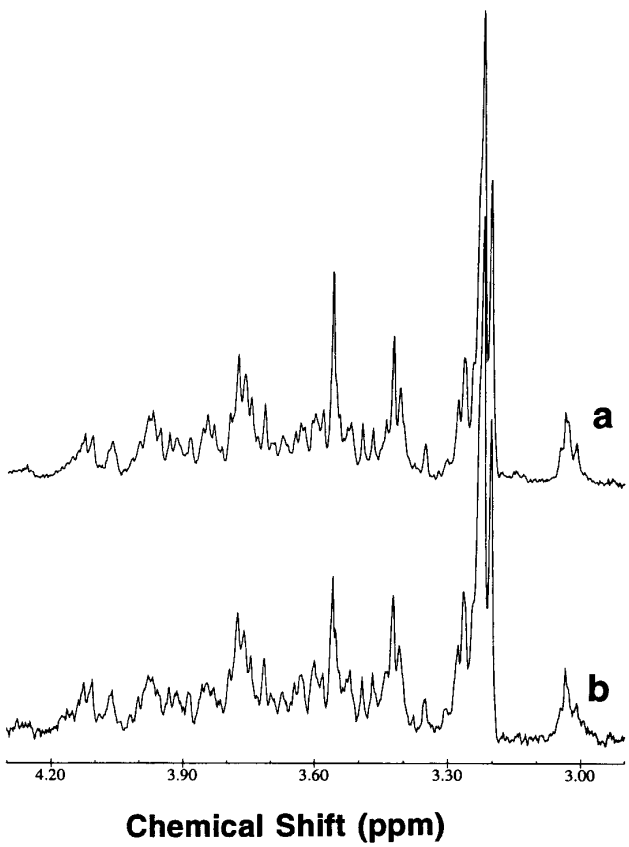

FIG. 3. HRMAS proton MR spectra of human breast specimen obtained from a patient diagnosed with grade II infiltrating ductal carcinoma and acquired two hours apart at 20°C.

Excess adipose tissue can prevent a meaningful estimation of absolute metabolic intensity as determined by sample weight. Therefore, to investigate the relationship between an increase in Pch and severity of ductal carcinomas and to compare results among cases, in Table 1, we have listed the percentage change of Pch intensity over the choline resonance intensity at 3.20 ppm. We further analyzed these Pch ratios as a function of ductal carcinoma grade, determined by histopathological evaluation of the adjacent site (see Experimental) as shown in Fig. 4a. This diagram suggests that the commonly observed bulk resonance of choline-related compounds arises largely from the Pch contribution in high grade carcinomas.

Lactate, a biochemical product of anaerobic respiration, has similarly been associated with the progression of malignancy, especially with the formation of necrosis. Lactate has been observed in *in vivo* MRS of various types of neoplastic diseases, such as human gliomas (*43, 44*). Fig. 4b depicts the ratio of lactate over choline, also found in Table 1, as a function of ductal carcinoma grade. However, to further our discussion of this diagram, we wish to emphasize that *ex vivo* analysis of lactate with intact tissues warrants extra caution, since lactate may be produced as a result of anaerobic biochemical reactions secondary to the excision of tissue from a living organ. Indeed, we observed this phenomena when lactate was recorded in the HRMAS spectrum of the healthy non-fatty breast tissue (Fig. 2b). Figure 4b, nevertheless, demonstrates that an increase in the lactate-to-choline ratio is positively correlated with an increase in tumor grade, and that this ratio may be used, with

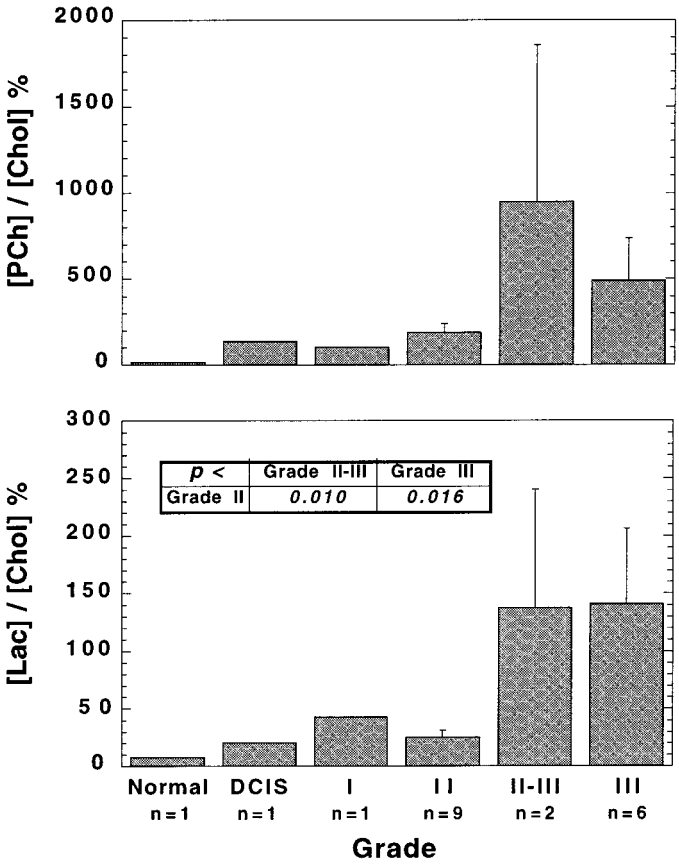

FIG. 4. Examples of observed correlations between histopathological grades of ductal carcinomas and the means for metabolic intensities measured with HRMAS 1HMRS method. Diagrams present correlation between tumor grades with (a) the relative intensity of phosphocholine (3.22 ppm) over choline (3.20 ppm), and (b) the relative intensity of lactate (4.12 ppm) over choline (3.20 ppm). Statistically significant variations of means that can differentiate between various tumor grades are labeled in the diagram.

statistical significance, to differentiate grade II ductal carcinomas from those of grade III. Our confidence in this correlation is based on: (1) results shown in Fig. 3, where we demonstrate that likely tissue degradation does not produce detectable spectral differences, including increases in lactate, within the HRMAS experimental time frame of 2 h, and (2) a correlation ($R = 0.57$, $p < 0.017$) observed between the lactate-to-choline ratio and the diameter of the primary tumors for 17 carcinoma cases. For these reasons, we believe that the observed increase in lactate relates directly to the severity of ductal carcinomas.

Table 3 analyzes the statistical significance of T2 variations in relation to ductal carcinoma grade. In clinical practice, significantly different T2 values can be used to develop T2 sensitive techniques that may assist with *in vivo* discrimination among different neoplasms. Table 3 demonstrates that a T2 increase in Pch may differentiate grade II from grade III ductal carcinomas, and that alterations in T2 among lipid components may be used to distinguish normals from carcinomas, as well as between carcinoma grades.

The above-discussed correlations between the mean of metabolic alterations and the ductal carcinoma grade illustrate the significant relationship between malignancy development and metabolic alterations. Analysis of tumor metabolites in individual cases may result in the establishment of independent evaluation parameters for future *in vivo* clinical use, with the potential of assessing tumor grade preoperatively.

In Fig. 5, we examine the metabolic alterations for individual carcinoma specimens, rather than collectively as a function of tumor grade. This figure reveals a linear correlation between Pch and lactate. We interpret this Pch-lactate correlation as an indication that the higher the PCh/Chol ratio in tumor, the higher the lactate content in tissue, due to the formation of necrosis during rapid tumor cell proliferation. The relationship demonstrated in Fig. 5 supports our discussion concerning the increases of Pch and lactate with regard to ductal carcinoma development. It also leads us to hypothesize that the metabolic relationship, such as that in Fig. 5, may provide a valuable measure not only for the clinical evaluation of ductal carcinomas, but also for differentiation between malignant breast cancer and benign breast diseases. Here, we wish to emphasize that although evaluation and characterization of benign breast diseases, such as fibrocystic changes, fibroadenomas, etc. (*50*), is an extremely important aspect in the clinic of human breast diseases, it was beyond the scope of this preliminary study. Nevertheless, our results here reported suggest that this new chemo-pathological approach may also be able to provide a sensitive measure in distinguishing benign vs malignancy, as long as there are metabolic differences between the two.

TABLE 3

Matrix of Selected Metabolic Spin–Spin Relaxation Time (T2) Measured with HRMAS 1HMRS for Differentiation between Different Pathological Specimens

	Normal ($n=4$)	II ($n=7$)	II-III ($n=2$)	III ($n=5$)
Normal		2.77* 1.30**	2.03** 1.30**	2.77* 2.03*
II			Pch (3.22)** 1.30*	Pch (3.22)**
II-III				1.30**
III				

Note. Numbers represent resonance chemical shift in ppm. Use of this matrix: As an example, T2 values of lipid resonances at 2.77, 2.03, and 1.30 ppm can be used to differentiate normal from various tumor groups with a significance of $p < 0.05$. Similarly the phosphocholine resonance (Pch), can be used to distinguish Grade II from Grade III with a $p < 0.05$ (indicated by **).

* $p < 0.05$ calculated according to 1-tailed Student's *t*-test, based on the hypothesis that T2 increases in tumors.

** $p < 0.05$ calculated according to 2-tailed Student's *t*-test.

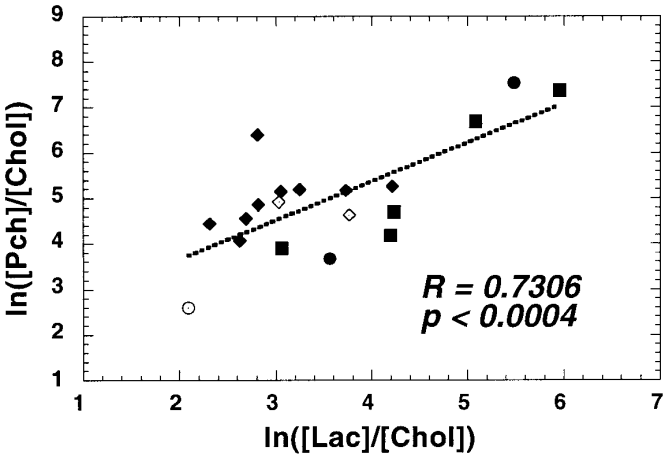

FIG. 5. Correlations between phosphocholine and lactate intensities measured from HRMAS 1HMR spectra for individual specimens of human ductal carcinomas (○, normal; ◇, DCIS and Grade I; ◆, Grade II; ●, Grade II-III; ■, Grade III), presented in natural log-scales.

CONCLUSIONS

In this report, we demonstrate that: (1) the intact tissue HRMAS 1HMRS technique is able to produce high-resolution spectra of specimens of human breast ductal carcinomas; (2) this novel spectroscopic technique provides a rapid, objective means of tumor evaluation; (3) normal may differentiate from carcinomas by cellular metabolism measured with HRMAS 1HMRS; and (4) tumor metabolism thus measured shows correlations with the overall tumor grade obtained from routine histopathological evaluation of the adjacent specimen. Although it is still an *ex vivo* methodology and relies on surgically removed specimens, HRMAS 1HMRS may provide information leading to the establishment of biochemical criteria that allow a more accurate diagnosis and prognosis of human breast cancer to be obtained. In addition to the potential utility of this technique in cancer diagnosis and prognostication, the capability that HRMAS 1HMRS confers for measurement of tumor metabolism in intact tissue may allow new *in vivo* diagnostic techniques, such as MR chemical shift imaging and *in vivo* spectroscopy, to be developed.

EXPERIMENTAL

The study was approved by the Subcommittee on Human Studies at the Massachusetts General Hospital.

Tissue Collection

Tissue specimens were dissected by pathologists less than 20 minutes after surgical resection and deep frozen in deuterated phosphate buffered saline (D2O/PBS) solution at −80°C until spectroscopy experiments were conducted. Ductal carcinoma specimens were obtained from the region adjacent to the sites that were histopathologically evaluated. Carcinoma-free tissues used as controls were collected from the margins of the resection, where no tumor cells were detected. Ductal carcinoma tissues from 19 female patients (age 33 to 85, mean 59.0 +/−3.3) were used in the study. Within this group, 18 cases were histopathologically diagnosed as grade I ($n = 1$), II ($n = 9$), II-III ($n = 2$), and III ($n = 6$). One case was diagnosed as ductal carcinoma-in-situ (DCIS).

An additional specimen of healthy human breast, also examined in this study, was generously provided by Dr. S. Singer of Boston Brigham and Women's Hospital.

1HMRS Experiments

All HRMAS 1HMRS studies were performed at 20°C on an MSL 400 NMR spectrometer (proton frequency at 400.13 MHz) by using a MAS probe modified for high-resolution (Bruker Instruments, Inc., Billerica, MA). A 7-mm MAS NMR rotor with two kel-f CRAMP inserts (Bruker Instruments, Inc. Billerica, MA) was used to hold tissue specimens, thawed for less than 10 minutes, that had been removed of both D2O/PBS and visible adipose tissue whenever possible. The MAS rate was stabilized at 2.500 (±0.001)kHz. Spectra presented here were acquired by using a rotor synchronized Carr-Purcell-Meibom-Gill (CPMG) pulse sequence [90–(τ–180–τ)$_n$–acquisition] as a T2-filter, to minimize spectral broadening due to lipids (*38*). The inter-pulse delay ($\tau = 2\pi/\omega_r = 400$ μs) was synchronized to the rotor rotation (τ represented the sample spinning speed in time unit, while $\omega_r/2\pi$ represented the MAS speed in kHz). The value for n was 500 ($2n\tau = 400$ ms). The 90° pulse length was adjusted for each sample independently and varied from 9.6 to 10.6 μs. The number of transients was 512, with an acquisition time of 1016 ms (16K complex points), a repetition time of 3.0 s, and a spectral width of 8 kHz (20 ppm). Before Fourier transformation and phasing, all free induction decays were subjected to 1Hz apodization. TMS at 0.00 ppm was used as an external chemical shift reference. With respect to TMS resonance, the internal references of lactate doublet were determined to be 1.32 and 1.34 ppm (*51*), which also led to a value of 0.9 ppm for the most up-field lipid resonance. No water suppression was used in HRMAS experiments. The resonance intensities of metabolites in tissue specimens were estimated based on the integration of resonance by using Lorentzian+Gaussian Curve-fitting in NMR1 (New Methods Research, Inc.).

Conventional 1HMR spectra were measured with a standard 5-mm probe. Tissue samples before and after MAS at 2.5 kHz were transferred to the 5-mm NMR tube and immersed in D2O/PBS solution. Glasswool was used at the bottom of the tube to adjust the sample to the coil active region. Low-power and continuous-wave water presaturation of 500 ms was used to remove water signal from PBS/D2O solution. Other than the use of a 90° pulse of 20 μs, all acquisition and processing conditions were the same as those described previously for HRMAS experiments.

ACKNOWLEDGMENTS

We are sincerely grateful to Mr. Sven D. Holder for his assistance in coordinating tissue collection. His persistent efforts contributed greatly to the success of this study. We thank Drs. F. C. Koerner, F. Fang, C. Mountford, and C. L. Lean for their collaboration and useful discussion and Ms. J. Fordham for her editorial assistance. This work was supported in part by an institutional grant from the American Cancer Society IRG-173H (LLC), in part by a Public Health Service Grant NS34626 (RGG), and in part by the MGH NMR Center.

REFERENCES

1. D. Adler and R. Wahl, New methods for imaging the breast: Techniques, finding, and potential, *Am. J. Roentgen.* **164,** 19–30 (1995).
2. K. Orang-Khadivi, B. Pierce, C. Ollom, L. Floyd, R. Siegle, and R. William, New magnetic resonance imaging techniques for the breast cancer, *Breast Cancer Res. Treat.* **32,** 119–135 (1994).
3. C. Hoh, C. Schiepers, M. Seltzer, S. Gambhir, D. Silverman, J. Czernin, J. Maddahi, and M. Phelps, PET in oncology: Will it replace the other modalities? *Semin. Nucl. Med.* **27,** 94–106 (1997).
4. P. Davis, M. Staiger, K. Harris, M. Ganott, J. Klementaviciene, J. McCarty, and H. Tobon, Breast cancer measurements with magnetic resonance imaging, ultrasonography, and mammography, *Breast Cancer Res. Treat.* **37,** 1–9 (1996).
5. H. Degani, V. Gusis, D. Weinstein, S. Fields, and S. Strano, Mapping pathophysiological features of breast tumors by MRI at high spatial resolution, *Nat. Med.* **3,** 780–782 (1997).
6. M. Hall-Craggs and H. Mumtaz, Keeping abreast of magnetic resonance: Developments in breast cancer imaging [editorial], *Clin. Radiol.* **52,** 253–255 (1997).
7. T. Helbich, A. Becherer, S. Trattnig, T. Leitha, P. Kelkar, M. Seifert, M. Gnant, A. Staudenherz, M. Rudas, G. Wolf, and G. Mostbeck, Differentiation of benign and malignant breast lesions: MR imaging versus Tc-99m sestamibi scintimammography, *Radiology* **202,** 421–429 (1997).
8. S. Mussurakis, D. Buckley, and A. Horsman, Dynamic MR imaging of invasive breast cancer: correlation with tumour grade and other histological factors, *Br. J. Radiol.* **70,** 446–451 (1997).
9. M. Sabel and H. Aichinger, Recent developments in breast imaging, *Phys. Med. Biol.* **41,** 315–368 (1996).
10. S. Graham, M. Bronskill, J. Byng, M. Yaffe, and N. Boyd, Quantitative correlation of breast tissue parameters using magnetic resonance and X-ray mammography, *Br. J. Cancer* **73,** 162–168 (1996).
11. E. Ranieri, M. D'Andrea, A. D'Alessio, S. Bergomi, G. Caprio, G. Calabrese, and F. Virno, Ultrasound in the detection of breast cancer associated with isolated clustered microcalcifications, mammographically identified, *Anticancer Res.* **17,** 2831–2835 (1997).
12. F. Hall, Technologic advances in breast imaging. Current and future strategies, controversies, and opportunities, *Surg. Oncol. Clin. N. Am.* **6,** 403–409 (1997).
13. S. Parker, T. Tong, S. Bolden, and P. Wingo, Cancer statistics, 1996, *CA* **46,** 5–27 (1996).
14. C. Furnival, Breast cancer: Current issues in diagnosis and treatment, *Aust. N. Z. J. Surg.* **67,** 47–58 (1997).
15. L. Tabar, P. Fagerberg, S. Duffy, N. Day, A. Gad, and O. Grontoff, Update of the Swedish two-county program of mammographic screening for breast cancer, *Radiol. Clin. N. Am.* **30,** 187–210 (1992).
16. R. Bettelheim, K. Price, R. Gelber, B. Davis, M. Castiglione, A. Goldhirsch, and A. Neville, The International (Ludwig) Breast Cancer Study Group: Prognostic importance of occult axillary lymph node micrometastases from breast cancer, *Lancet* **335,** 1565–1568 (1990).
17. M. Kaufmann, Review of known prognostic variables, *Rec. Results Cancer Res.* **140,** 77–87 (1996).
18. M. Pack and R. Thomas, Axillary lymph node dissection: Does it have a role in primary breast cancer? *Am. Surg.* **62,** 159–161 (1996).
19. B. Fisher, F. Perera, A. Cooke, A. Opeitum, V. Venkatesan, A. Dar, and L. Stitt, Long-term follow-up of axillary node-positive breast cancer patients receiving adjuvant systemic therapy alone: alone: Patterns of recurrence, *Int. J. Radiat. Oncol. Biol. Phys.* **38,** 541–550 (1997).
20. M. Shetty and J. Reiman HM, Tumor size and axillary metastasis, a correlative occurrence in 1244 cases of breast cancer between 1980 and 1995, *Eur. J. Surg. Oncol.* **23,** 139–141 (1997).
21. J. Simpson and D. Page, The role of pathology in premalignancy and as a guide for treatment and prognosis in breast cancer, *Semin. Oncol.* **23,** 428–435 (1996).
22. C. Mountford, C. L. Lean, W. Mackinnon, and P. Russell, The use of proton MR in cancer pathology, *in* "Annual Report on NMR Spectroscopy" (G. Webb, Ed.) , pp. 173–215, Academic Press, London (1993).
23. D. Leibfritz, An introduction to the potential of 1H-, 31P- and 13C-NMR-spectroscopy, *Anticancer Res.* **16,** 1317–1324 (1996).
24. J. de Certaines, High resolution nuclear magnetic resonance spectroscopy in clinical biology: application in oncology, *Anticancer Res.* **16,** 1325–1332 (1996).
25. C. Mountford, C. Lean, R. Hancock, S. Dowd, W. Mackinnon, M. Tattersall, and P. Russell, Magnetic resonance spectroscopy detects cancer in draining lymph nodes, *Invasion Metastasis* **13,** 57–71 (1993).
26. O. Kaplan, T. Kushnir, N. Askenazy, T. Knubovets, and G. Navon, Role of nuclear magnetic resonance spectroscopy (MRS) in cancer diagnosis and treatment: 31P, 23Na, and 1H MRS studies of three models of pancreatic cancer, *Cancer Res.* **57,** 1452–1459 (1997).
27. A. Kuesel, T. Kroft, J. Saunders, M. Prefontaine, N. Mikhael, and I. Smith, A simple procedure for obtaining high-quality NMR spectra of semiquantitative value from small tissue specimens: Cervical biopsies, *Magn. Reson. Med.* **27,** 340–355 (1992).
28. P. Williams, J. Saunders, M. Dyne, C. E. Mountford, and K. Holmes, Application of a T2-filtered COSY experiment to identify the origin of slowly relaxing species in normal and malignant tissue, *Magn. Reson. Med.* **7,** 463–471 (1988).
29. A. Kuesel, G. Sutherland, W. Halliday, and I. Smith, 1H MRS of high grade astrocytomas: mobile lipid accumulation in necrotic tissue, *NMR Biomed.* **7,** 149–155 (1993).
30. A. Rutter, H. Hugenholtz, J. Saunders, and I. Smith, Classification of brain tumors by ex vivo 1H NMR spectroscopy, *J. Neurochem.* **64,** 1655–1661 (1995).
31. R. Somorjai, B. Dolenko, A. Nikulin, N. Pizzi, G. Scarth, P. Zhilkin, W. Halliday, D. Fewer, N. Hill, I. Ross, M. West, I. Smith, S. Donnelly, A. Kuesel, and K. Briere, Classification of 1H MR spectra of human brain neoplasms: The influence of preprocessing and computerized consensus diagnosis on classification accuracy, *J. Magn. Reson. Imaging* **6,** 437–444 (1996).
32. C. Lean, R. Newland, D. Ende, E. Bokey, I. Smith, and C. Mountford, Assessment of human colorectal biopsies by 1H MRS: Correlation with histopathology, *Magn. Reson. Med.* **30,** 525–533 (1993).
33. P. Russell, C. Lean, L. Delbridge, G. May, S. Dowd, and M. CE, Proton magnetic resonance and human thyroid neoplasia. I: Dis-

crimination between benign and malignant follicular thyroid neoplasmas by magnetic resonance spectroscopy, *Am. J. Med.* **96,** 383–388 (1994).

34. L. Delbridge, C. Lean, P. Russell, G. May, S. Roman, S. Dowd, T. Reeve, and C. Mountford, Proton magnetic resonance and human thyroid neoplasia. II: Potential avoidance of surgery for benign follicular neoplasms, *World J. Surg.* **18,** 512–517 (1994).

35. A. Fowler, A. Rappas, J. Holder, A. Finkbeiner, G. Dalrymple, M. Millins, J. Sprigg, and R. A. Komoroski, Differentiation of human prostate cancer from benign hypertrophy by in vitro 1H NMR, *Magn. Reson. Med.* **25,** 140–147 (1992).

36. W. Mackinnon, P. Barry, P. Malycha, D. Gillett, P. Russell, C. Lean, S. Doran, B. Barraclough, M. Bilous, and C. Mountford, Fine-needle biopsy specimens of benign breast lesions distinguished from invasive cancer ex vivo with proton MR spectroscopy, *Radiology* **204,** 661–666 (1997).

37. L. L. Cheng, I. W. Chang, D. A. Louis, and R. G. Gonzalez, Correlation of high resolution magic angle spinning proton MR spectroscopy with histopathology of intact human brain tumor specimens, *Cancer Res.* **58,** 1825–1832 (1998).

38. L. L. Cheng, C. Lean, A. Bogdanova, J. Wright, SC, J. Ackerman, T. Brady, and L. Garrido, Enhanced resolution of proton NMR spectra of malignant lymph nodes using magic-angle spinning, *Magn. Reson. Med.* **36,** 653–658 (1996).

39. D. Moka, R. Vorreuther, H. Schicha, M. Spraul, E. Humpfer, M. Lipinski, P. Foxall, J. Nicholson, and J. Lindon, Magic angle spinning proton nuclear magnetic resonance spectroscopic analysis of intact kidney tissue samples, *Anal. Commun.* **34,** 107–109 (1997).

40. K. Millis, W. Maas, D. Cory, and S. Singer, Gradient, high-resolution, magic-angle spinning nuclear magnetic resonance spectroscopy of human adipocyte tissue, *Magn. Reson. Med.* **38,** 399–403 (1997).

41. P. Weybright, K. Millis, N. Campbell, D. G. Cory, and S. Singer, Gradient, high-resolution magic-angle spinning 1H nuclear magnetic resonance spectroscopy of intact cells, *Magn. Reson. Med.* **39,** 337–344 (1998).

42. L. L. Cheng, M. Ma, L. Becerra, T. Ptak, I. Tracey, A. Lankner, and R. Gonzalez, Quantitative neuropathology by high resolution magic angle spinning proton magnetic resonance spectroscopy, *Proc. Natl. Acad. Sci. USA* **94,** 6408–6413 (1997).

43. K. Herholz, W. Heindel, P. Luyten, J. den Hollander, U. Pietrzyk, J. Voges, H. Kugel, G. Friedmann, and W. Heiss, In vivo imaging of glucose consumption and lactate concentration in human gliomas, *Ann. Neurol.* **31,** 319–327 (1992).

44. M. Preul, Z. Caramanos, D. Collins, J.-G. Villemure, R. Leblanc, A. Olivier, R. Pokrupa, and D. Arnold, Accurate, noninvasive diagnosis of human brain tumors by using proton magnetic resonance spectroscopy, *Nature Med.* **2,** 323–325 (1996).

45. F. Podo and J. de Certaines, Magnetic resonance spectroscopy in cancer: Phospholipid, neutral lipid and lipoprotein metabolites and function, *Anticancer Res.* **16,** 1305–1316 (1996).

46. H. Degani, Biological and physiological basis of breast MR, *in* "Proceedings of the International Society for Magnetic Resonance in Medicine 4th Scientific Meeting and Exhibition, New York, 1996," p. 333.

47. L. Le Moyec, R. Tatoud, M. Eugene, C. Gauville, I. Primot, D. Charlemagne, and F. Calvo, Cell and membrane lipid analysis by proton magnetic resonance spectroscopy in five breast cancer lines, *Bri. J. Cancer* **66,** 623–628 (1992).

48. S. Singer, K. Souza, and W. Thilly, Pyruvate utilization, phosphocholine and adenosine triphosphate (ATP) are markers of human breast tumor progression: A 13P- and 13C-nuclear magnetic resonance (NMR) spectroscopy study, *Cancer Res.* **55,** 5140–5145 (1995).

49. Y. Ting, D. Sherr, and H. Degani, Variations in energy and phospholipid metabolism in normal and cancer human mammary epithelial cells, *Anticancer Res.* **16,** 1381–1388 (1996).

50. C. Elston and I. Ellis, "Systemic Pathology: The Breast," 3rd ed., Vol. 13, Churchill Livingstone, Edinburgh (1998).

51. D. Sze and O. Jardetzky, Determination of metabolite and nucleotide concentrations in proliferating lymphocytes by 1H-NMR of acid extracts, *Biochim. Biophys. Acta* **1054,** 181–187 (1990).